Supporting Materials:

Microbial Control of Sea Spray Aerosol Composition: A Tale of Two Blooms

Xiaofei Wang[1**], Camille M. Sultana[1**], Jonathan Trueblood[2], Thomas C. J. Hill[3], Francesca Malfatti[4,5], Christopher Lee[1], Olga Laskina[2], Kathryn A. Moore[1], Charlotte M. Beall[4], Christina S. McCluskey[3], Gavin C. Cornwell[1], Yanyan Zhou[4,6], Joshua L. Cox[1], Matthew A. Pendergraft[4], Mitchell V. Santander[1], Timothy H. Bertram[7], Christopher D. Cappa[8], Farooq Azam[4], Paul J. DeMott[3], Vicki H. Grassian[2] and Kimberly A. Prather[1]*

[1] Department of Chemistry and Biochemistry
University of California, San Diego
La Jolla, CA 92093, U.S.A.
[2] Department of Chemistry
University of Iowa
Iowa City, IA 52242, U.S.A
[3] Department of Atmospheric Science
Colorado State University
Fort Collins, CO 80523, U.S.A.
[4] Scripps Institution of Oceanography
University of California, San Diego
La Jolla, CA 92093, U.S.A
[5] National Institute of Oceanography and Experimental Geophysics,
Trieste 34100, Italy
[6] State Key Laboratory of Marine Environmental Science and Key Laboratory of the MOE for Coastal and Wetland Ecosystems, School of Life Sciences,
Xiamen University
Xiamen 361005, PR China
[7] Department of Chemistry
University of Wisconsin–Madison
Madison, WI 53706, U.S.A.
[8] Department of Civil and Environmental Engineering
University of California, Davis
Davis, CA 95616, U.S.A.

*To whom correspondence should be addressed.
**These authors have an equal contribution.
Correspondence to: Kimberly A. Prather
Email: kprather@ucsd.edu , Tel: 1- 858-822-5312

Pages: 25

Tables: 1

Figures: 8

SUPPORTING INFORMATION

METHOD

S1. General Experiment Summary

Natural phytoplankton blooms were initiated in a wave channel in July 2014. Nutrients were added to natural seawater that was illuminated continuously to stimulate phytoplankton growth. SSA particles were generated through wave breaking and measured continuously throughout the course of the experiments. Chemical and biological bulk seawater measurements were also taken daily. Details of the experimental methods are given below.

S2. Water Collection

All seawater was collected from Scripps Pier (La Jolla, CA; 32°51´56.8"N: 117° 15´38.48"W) and filtered through a 50 μm mesh to remove debris and zooplankton before addition to the wave channel. The pump inlet was at least 5 meters below the surface of the water. The table below summarizes collection times and volumes for the experiment.

Table S1.

Experiment	**Date**	**Time**	**Volume**	**t = 0 for plots**
Wave channel	7/3/14	7:00-16:00	13000 L	7/3/14 10:00:00

S3. Nutrient Addition

All experiments used f/2 algae growth medium (Proline, Aquatic Eco-Systems, Apopka, FL) in addition to solutions of sodium metasilicate. Species concentrations have been detailed in previous work.[1] An additional 9 μM sodium phosphate was added to the wave flume on 7/25/14 01:00 to maintain enriched levels of phosphate. .

S4. Wave Channel Set-up

Nutrients were added simultaneously with the freshly collected seawater to ensure adequate mixing. The wave channel was illuminated continuously for the entirety of the experiment with 5700 K full spectrum lights. Measurement of photosynthetically active radiation (PAR) within the wave channel was roughly 45 μE m^{-2} s^{-1}. To ensure low background particle counts and clean conditions, hydrocarbon, oxidant, and particle filtered air was delivered to the headspace of the channel with an average along-channel airflow velocity of approximately 5 cm s^{-1}. Breaking waves were used to generate SSA. The aerosol sampling manifold was approximately 4 feet from the location where the waves broke. Details of the air handling system and wave generation mechanism have been previously described.[2,3] Bulk seawater samples were collected daily between where the waves broke and the aerosol sampling manifold and at least 6 inches below the water surface.

S5. Bulk Seawater Measurements

Bulk chlorophyll-a concentrations were measured fluorometrically using a Wetlabs ECO BBFL2 sensor and Turner AquaFluor handheld unit. The Wetlabs sensor was integrated into a flow-through system with a pump, housing, and additional sensors for continuous measurements; the AquaFluor was used with discrete samples. The Wetlabs sensor was calibrated at the factory against *T. weissflogii* cultures, and used as received. Measurements made with the AquaFluor were calibrated against simultaneous values recorded by the Wetlabs sensor, and then the two datasets were combined into a single timeseries.

Heterotrophic bacteria and viruses were enumerated via epifluorescence microscopy (Keyence BZ-X700) with SYBR Green-I nucleic acid gel stain (Life Technologies, S-7563).[4] Seawater samples were pipetted into sterile cryogenic vials and preserved with 0.05% electron microscopy grade glutaraldehyde. After incubation at 4 ºC for 15 min, samples were flash frozen in liquid nitrogen and then stored at -80 °C until analysis.

The fluorogenic substrate method was used to measure the enzymatic activities of lipase, protease, alkaline phosphatase and chitinase.[5] All the substrates (Sigma-Aldrich) were used to a

final concentration of 20 μM.[6] Lipase activity was measured using 4-Methyl-umbelliferone oleate and 4-Methyl-umbelliferone stearate. Protease was measured using L-Leucine-7-amino-4-methyl-coumarin. The alkaline phosphatase activity was measured using 4-Methyl-umbelliferone-phosphate. The chitinase activity was measured using 4-methyl-umbelliferone-N-acetyl-β-D-glucosaminide. After the addition of the substrate, the samples were incubated at the *in situ* temperature in the dark for one hour. Assays were performed in microtiter plates (SpectraMax M3, Molecular Device) in triplicate. Fluorescence was measured immediately after adding substrates and again at the end of the incubation,[7] at 355/460 nm (excitation/emission). The fluorescence signal after blank correction was calibrated against 4-MUF and 7-AMC standards. The activities were computed as nmol substrate hydrolyzed L^{-1} h^{-1}.

S6. Measurement of Aerosol Size Distributions

Aerosol size distributions were measured using a Scanning Mobility Particle Sizer (SMPS, TSI Inc. Model 3936) and Aerodynamic Particle Sizer (APS, TSI Inc. Model 3321). SMPS measurements were made of particles with dry (RH<40%) mobility diameters (D_m) in the range 0.013-0.750 μm; assuming sphericity implies the measured D_m is equivalent to physical diameter (D_p). APS measurements were adjusted from aerodynamic diameter (D_a) to D_p assuming spherical particles with an effective density of 1.8 g cm^{-3}.[8] After density adjustment, APS measurements were of particles with dry (RH<40%) D_p in the range 0.460-17.930 μm. SMPS and APS (after adjustment) distributions were merged at a diameter of 0.540 μm, with SMPS sizes greater and APS sizes smaller than the cutoff being truncated. Size distributions were used to estimate $[PM_1]_{dry}$ by integrating the merged distribution up to 1 μm and calculating the expected mass, again assuming particle sphericity and an effective density of 1.8 g cm^{-3}.

S7. Measurement of SSA Composition via An Aerosol Time-of-flight Mass Spectrometer (ATOFMS)

The chemical composition of individual SSA particle (D_{va} = 0.25-3 μm, vacuum aerodynamic diameter) was measured in real time via ATOFMS which yielded dual-polarity mass spectra. As particle phase water has been shown to reduce the negative ion signal,[9] the sampled SSA passed through a silica gel diffusion dryer before the instrument inlet. A brief description of the ATOFMS follows here; more detailed discussion of the ATOTMS has been provided previously.[10,11] Aerosol particles enter the instrument through a converging nozzle inlet and are then accelerated to their size-dependent terminal velocity in a differentially pumped vacuum chamber. The time for particles to transit two continuous wave laser beams (532 nm) that are separated by a fixed distance is measured. A calibration with polystyrene latex spheres of known diameter is used to convert the velocity to vacuum aerodynamic diameter. The velocity of the particles is used to trigger a pulsed, Q-switched, UV desorption-ionization laser. The particle's chemical components are desorbed and ionized in the ion source region by the Nd:YAG laser (266 nm, 8 ns, 1.3 mJ) pulse. The positive and negative ions produced are detected by a dual-polarity reflectron time-of-flight mass spectrometer.

Single particle spectra and size data were loaded into Matlab (The MathWorks, Inc.) and analyzed via the software toolkit YAADA (http://www.yaada.org/). Particles were divided into clusters based on their spectra via an adaptive neural network (ART-2a) and the resultant clusters were recombined into types based on their characteristic mass spectra and size distributions.[12]

S8. Measurement of SSA Composition via A High-resolution Aerosol Mass Spectrometer (AMS)

SSA produced from the wave channel were first dried by a diffusional dryer, and then introduced into an AMS, which is equipped with a high resolution time-of-flight mass spectrometer. Its detailed description can be found in DeCarlo et al.[13] A brief introduction to the AMS is given here. Aerosol particles (D_{va} = 0.04 ~ 1 μm) can efficiently enter the AMS through an aerodynamic lens, which focuses particles into a narrow beam. Noticeably, the AMS also samples some supermicron particles although with a relatively low collection efficiency,[14,15]

especially when the total aerosol mass is mainly located in the supermicron size range, as is the case for SSA in this study (Figure S8). Next, particles are resolved based on their measured velocities, which are used to calculate their vacuum aerodynamic particle diameters. Then, particles are collected on a hot vaporizer (set to 600 °C) where organics and other non-refractory matter are vaporized. Electron impact ionization is used to ionize the vapor and produce ions, which are analyzed by a mass spectrometer. The organic signals at m/z 28 and 44 were adjusted based on the CO_2 concentration in air, which was monitored by a CO_2 gas analyizer (Model LI-820, LI-COR, Inc., Nebraska, USA). The exact ion formula of peaks (e.g. $C_xH_yO_z$) were calculated based on their accurate mass. Overall elemental ratios for all organic signals were also obtained.[16]

The AMS measured dry vacuum aerodynamic particle diameter. Assuming the SSA were spherical, their density (ρ) was 1.8 g/cm^3, and their growth factor (GF) at a relative humidity (RH) of 80% was 2,[17] the aerodynamic diameter at RH 80% was calculated based on the relationship between vacuum aerodynamic particle diameter (D_{va}) and aerodynamic diameter (D_a)[13]:

$$D_{a@RH\ 80\%} = GF_{@RH\ 80\%} \times D_{a,dry} = GF_{@RH\ 80\%} \times D_{va,dry}/SQRT(\rho)$$

The AMS data were loaded into Igor Pro (Wavemetrics) and analyzed using SQUIRREL and PIKA, which are the standard AMS data analysis toolkits. Postive matrix factorization (PMF) technique[18,19] was applied to the high resoluion organic signals from the V-mode. The data for PMF was pre-treated, including removing the organic peaks with a signal-to-noise ratio (SNR) < 0.2, down-weighting the peaks (0.2 < SNR < 2), and further down-weighting the peaks with duplicated information related to CO_2^+. The total AMS organic signals were seperated into two PMF factors: the aliphatic-rich (AR) factor and oxygen-rich (OR) factor.

In the paper, f_{OM} is defined as the relative organic mass fraction of SSA:

$$f_{OM} = \left[\frac{[OM]}{[PM_1]_{dry}}\right] / \left[\frac{[OM]}{[PM_1]_{dry}}\right]_{max}$$

f_{AR} and f_{OR} are defined as the relative aliphatic-rich factor or oxygen-rich factor mass concentrations, respectively:

$$f_{AR} = \left[\frac{[AR]}{[PM_1]_{dry}}\right] / \left[\frac{[OM]}{[PM_1]_{dry}}\right]_{max}$$

$$f_{OR} = \left[\frac{[OR]}{[PM_1]_{dry}}\right] / \left[\frac{[OM]}{[PM_1]_{dry}}\right]_{max}$$

where [OM] is the total AMS organic signal. [AR] and [OR] are the aliphatic-rich (AR) factor and oxygen-rich (OR) factor, respectively. $[PM_1]_{dry}$ is the dry sub-micrometer particulate mass concentration estimated from the size distributions. "max" means maximum value.

S9. Measurement of SSA Composition Using Micro-Raman Spectroscopy

Individual SSA particles were collected on quartz discs (Ted Pella Inc., part no. 16001-1) placed on different stages of a Micro-Orifice Uniform Deposition Impactor (MOUDI, MSP Corp. Model 110) operating at a flow rate of 30 LPM, at RH ~72%. Particles collected on the the fourth stage, with aerodynamic diameters between 1.8 and 3.2 μm, and the sixth stage, with aerodynamic diameters between 0.56 and 1 μm, were analyzed. A LabRam HR Evolution Raman spectrometer (Horiba) with a 530 nm laser (30 mW) was used with a laser exposure time of 5-10 s. Two successive exposures were averaged to obtain each individual particle spectrum.

The sample for Raman data shown in this paper was taken 1:12 pm-2:06 pm (Local Time) on July 17, 2014 (day 14), while the AMS was sampling from 9-11am, 1-4 pm and 6-9 pm (Local Time) on this day.

Particles that contained Raman peaks associated with organic compounds were further analyzed and compared to representative standards. For example, the spectrum shown in Figure S6A has prominent peaks in the C-H stretching region at 2846 and 2880 cm^{-1} that correspond to symmetric and asymmetric stretches of the CH_2 group respectively. Additional peaks of lower intensity are associated with C-C stretching (1062 cm^{-1}, 1129 cm^{-1}), CH_2 twisting (1295 cm^{-1}) and bending (1439 cm^{-1} and 1461 cm^{-1}) modes.[20-24] These spectra have been compared to spectra of saturated fatty acids with chain lengths between 12 and 18. Spectra of all standard acids are very similar with prominent peaks. Based on this comparison, the Raman spectra shown in Figure S6A are assigned to long chain fatty acids with a chain length between 12 and 18. From

this analysis, the oxygen to carbon ratio (O/C) is between 0.11 and 0.17. These molecular species are referred to as "low O/C" species.

The Raman spectrum shown in Figure S6B features four peaks in the CH stretching region (2915 cm^{-1}, 2936 cm^{-1}, 2985 cm^{-1}, 2998 cm^{-1}), a large 3408 cm^{-1} peak due to OH stretch, stretching vibrations of C-O and C-C bonds characteristic of the carbohydrate nature (1009 cm^{-1}, 1037 cm^{-1}, 1097 cm^{-1}), bending deformations of COH group (867 cm^{-1}) and CH_2 and CH_2OH groups (1310 cm^{-1}, 1363 cm^{-1}, 1428 cm^{-1}, 1452 cm^{-1}, 1475 cm^{-1}) as well as amide I and III bands at 1250 cm^{-1} and 1640 cm^{-1} respectively.[20,25-28] This spectrum can be compared to spectra associated with carbohydrates typically found in the marine environment.[29-34] In particular, carbohydrate model compounds analyzed with Raman spectroscopy have similar characteristic peaks in the C-H stretching region although some of the relative intensities of these peak can differ. Based on the peak assignments and comparison to standard spectra, this SSA particle is associated with carbohydrates. Some common carbohydrates in the marine environment include ribose (O/C=1), heptose (O/C=1), glucose (O/C=1), glucosamine (O/C=0.83), fucose (O/C=0.83), mannose (O/C=1), galactose (O/C=1), and sialic acid (O/C=0.82).[29-34] These carbohydrates all have oxygen to carbon ratios between 0.82 and 1 and therefore are referred to as "high O/C" species.

A third particle type gives a Raman spectrum that is shown in Figure S6C. The Raman peaks in this spectrum are identified as a having skeletal C-C, C-O and stretching C-C-O bands at 991 cm^{-1} and 1044 cm^{-1}, CH_2 bending modes at 1459 cm^{-1} that is common for proteins and lipids, a peak at 1642 cm^{-1} that can be assigned as either an amide I band or C=C stretching vibration of unsaturated fatty acid chains, and a broad peak at 2929 cm^{-1} identified as the C–H stretching modes of CH, CH_2 and CH_3 groups of fatty acid chains.[35,36] This spectrum compares well with the spectrum of commercially available lipopolysaccharide (LPS) derived from *E. coli*. Indeed spectra of E. coli LPS features similar peaks and therefore, based on the peak assignments and comparison with standards, the type of spectra shown in Figure S6C has been associated with LPS. LPS consist of approximately 70% carbohydrates and 30% fatty acids.[37,38] Assuming the O/C ratio of carbohydrates is 0.85 and O/C ratio of fatty acids is 0.15 (*vide supra*) it can be inferred that the O/C ratio of LPS is approximately 0.6. Using a cutoff of 0.5, to identify "low" and "high" oxygen to carbon ratio containing molecules, LPS here is referred to as a "high O/C" species.

In addition to these three most common types of particles identified by the Raman spectra shown in Figure S6, other types of particles were either highly fluorescent under the laser beam during data collection or had uncommon organic signatures that did not allow them to be characterized or grouped further. These particles collectively accounted for 6% and 19% of total particles measured in the submicron and supermicron size range, respectively.

S10. Measurement of Ice Nucleating Particles (INP) with Colorado State University's Ice Spectrometer (CSU-IS)

Samples were obtained by filtering between 6-7 L min^{-1} of flume headspace air for 3-7 h through a 47 mm diameter in-line aluminum filter holder (Pall) fitted with a 0.05 μm diameter pore Nuclepore polycarbonate membrane (Whatman). A 3 μm Nuclepore membrane was placed below the sampling membrane as an additional cleanliness measure. Filter holders were cleaned between events, after disassembly, by soaking in 10% H_2O_2 for 60 min followed by three rinses in deionized water (18 MΩ and 0.2 μm diameter-pore filtered) and removal of excess water with a gas duster before drying. Filters were cleaned and any contaminating DNA removed by soaking in 10% H_2O_2 for 10 min in a sterile, 150 mm petri dish (CELLTREAT) followed by three rinses in deionized water, the last of which had been filtered through a 0.02 μm pore diameter filter (Anotop 25 mm syringe filter, Whatman). Filters were then dried on foil. Cleaning and drying were performed in a laminar flow cabinet (<0.01 particles mL^{-1}).

After particle collection, filters were transferred using clean, acetyl plastic forceps (Fine Science Tools) to sterile, 60 mm petri dishes (CELLTREAT) and stored at -20°C until processed. For the release of particles, filters were placed in sterile 50 mL Falcon polypropylene tubes (Corning Life Sciences), 5 mL of deionized water (18 MΩ and 0.2 μm diameter-pore filtered with ~2 INP mL^{-1} at -22°C) added and particles re-suspended by tumbling end-over-end on a Roto-Torque (Cole-Palmer) at 60 cycles min^{-1} for 20 min. To assess the heat labile fraction, 1.8 mL of the suspension solution was transferred to a 50 mL Falcon centrifuge tube and immersed in water heated to 95°C for 20 min (after allowing time for equilibration). Immersion freezing temperature spectra of INP were obtained using 24-32 aliquots of 50 or 60 μL dispensed into sterile, 96-well polymerase chain reaction (PCR) trays (LS-9796, Life Science Products Inc.) in a laminar flow cabinet. Trays were capped with polystyrene lids (Nunc microwell plates, Thermo Fisher Scientific Inc.) and then transferred to the CSU-IS. Based on aliquot size and number, the

detection limit for INP was calculated to be 0.001 L^{-1} and 0.002 L^{-1} air in untreated and heated sample experiments, respectively.

The CSU-IS is constructed using two 96-well aluminum incubation blocks (VWR), designed for cooling or heating PCR plates, placed end-to-end and encased on their sides and base by cold plates (Lytron). A ULT-80 low temperature bath (Thermo Neslab) circulating SYLTHERM XLT heat transfer fluid (Dow Corning Corporation) is used for cooling the plates via copper coils. Loaded PCR plates were placed in the blocks, the device covered with a plexiglass window and the headspace purged with 1.5 L min^{-1} of filtered (HEPA-CAP, Whatman) nitrogen. Temperature was then lowered at 0.33°C min^{-1}, and measured using a thermistor verification probe (Bio-Rad, Hercules, CA, VPT-0300) inserted into a side well. Temperature uncertainty was ±0.2°C, mostly from temperature variation across the blocks due to gradients in cooling. Frozen wells were counted at 0.5 or 1°C degree intervals, and cumulative numbers of INP mL^{-1} of suspension estimated using the formula $\ln(f)/V$, where f is the proportion of droplets not frozen and V is the volume of each aliquot.[39] This was converted to INP L^{-1} air using the volume of air filtered. Filter blanks were used to obtain a mean background INP spectrum.

Binomial sampling confidence intervals (95%) were derived using the following formula:[40]

$$\mathrm{CI}_{95\%} = \left(\hat{p} + \frac{1.96^2}{2n} \pm 1.96 \sqrt{\left[\hat{p}(1-\hat{p}) + {1.96^2}/{4n} \right]/n} \right) / \left(1 + {1.96^2}/{n} \right),$$

where $\hat{p}$ is the proportion of droplets frozen and n is the total number of droplets.

S11. Calculating Labile Organic Species in Seawater during the Mesocosm Experiment

For these calculations, it is assumed that aliphatic-rich labile organic species (ARL) are only produced by phytoplankton and transformed by lipase enzyme activity. Below is a list of assumptions:

(1) The production rate of ARL is linearly dependent on the concentration of phytoplankton. Thus the production rate can be expressed in the following form: d[ARL]/dt = k^+[Chl_a], where k^+ is a first-order reaction constant.

(2) The transformation of ARL follows Michaelis–Menten kinetics: d[ARL]/dt = R_max × [ARL] / ($C_{1/2}$ + [ARL]), where R_max is the maximum transformation rate of ARL. $C_{1/2}$ is the ARL concentration at half of its maximum transformation rate.

(3) The lipase activity was measured (shown in Figure 3) based on the decomposition rate of MUF-oleate at a saturating concentration (Method S12) in nM h^{-1}. However, phytoplankton produced ARL must include non-oleate compound lipids. Thus, in this model, only the trend of the lipase activity is used with units of au/day (au means arbitrary unit).

Therefore, the governing equation of ARL concentration takes the following form:

$$\frac{d[\mathrm{ARL}]}{dt} = k^{+}[Chl\_a] - R_{max} \cdot [\mathrm{ARL}]/(C_{1/2} + [\mathrm{ARL}])$$

There are 3 rate constants in the above equation: k^+, R_max and $C_{1/2}$. k+ and $C_{1/2}$ are unknown. The concentration of Chl-a and R_max are known and input into the model from measurements during the mesocosm.

SUPPORTING FIGURES

Figure S1. Schematic drawing of the IMPACTS experiment set-up

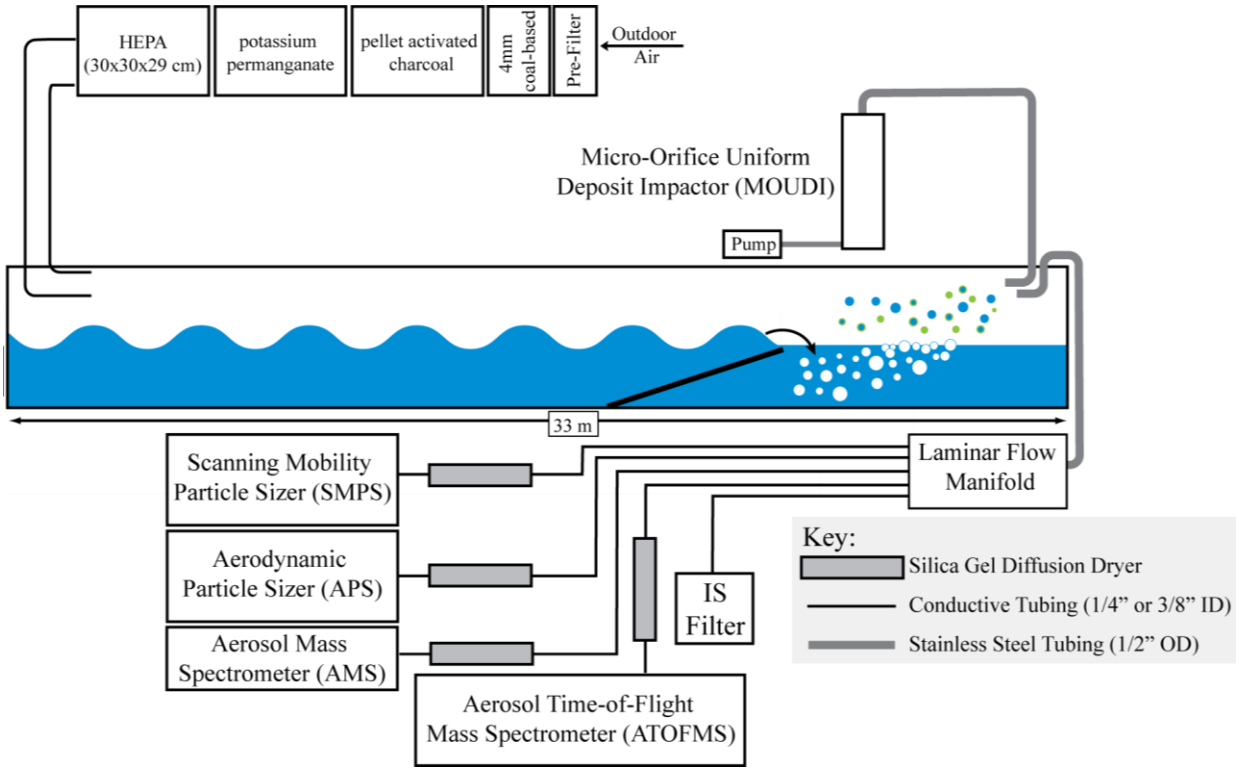

Figure S2. Size resolved organic AMS spectra of SSA from the wave-channel: The major peaks in the mass spectrum for the submicron mode are 43, 55, 57, 79, 81 and 83, which are typical hydrocarbon fragments.[41] Since the concentration of pure hydrocarbon in natural unpolluted seawater is low,[42] the organic species in this mode were likely molecules with long hydrocarbon chains, such as lipids. Conversely, the mass spectrum for particles in the supermicron mode shows a large peak at m/z 44 and m/z 28, indicators of oxidized organic matter. The hydrocarbon peaks were much smaller compared to those in the submicron mode.

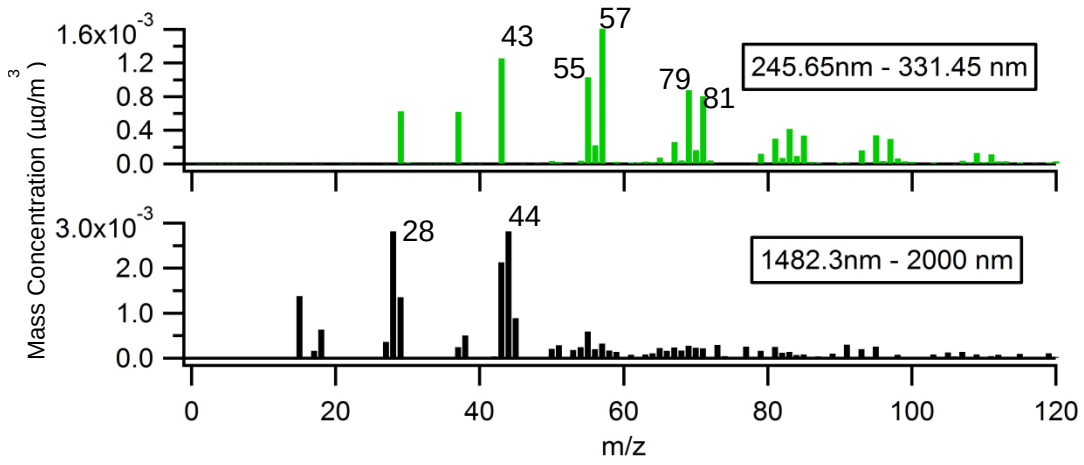

Figure S3. AMS organic spectrum of bulk seawater (**last panel**). Seawater from the wave channel was atomized to produce droplets, which were then dried and sampled by the AMS. All other AMS spectra used in this study (including Figure 2B and S2) are compared here.

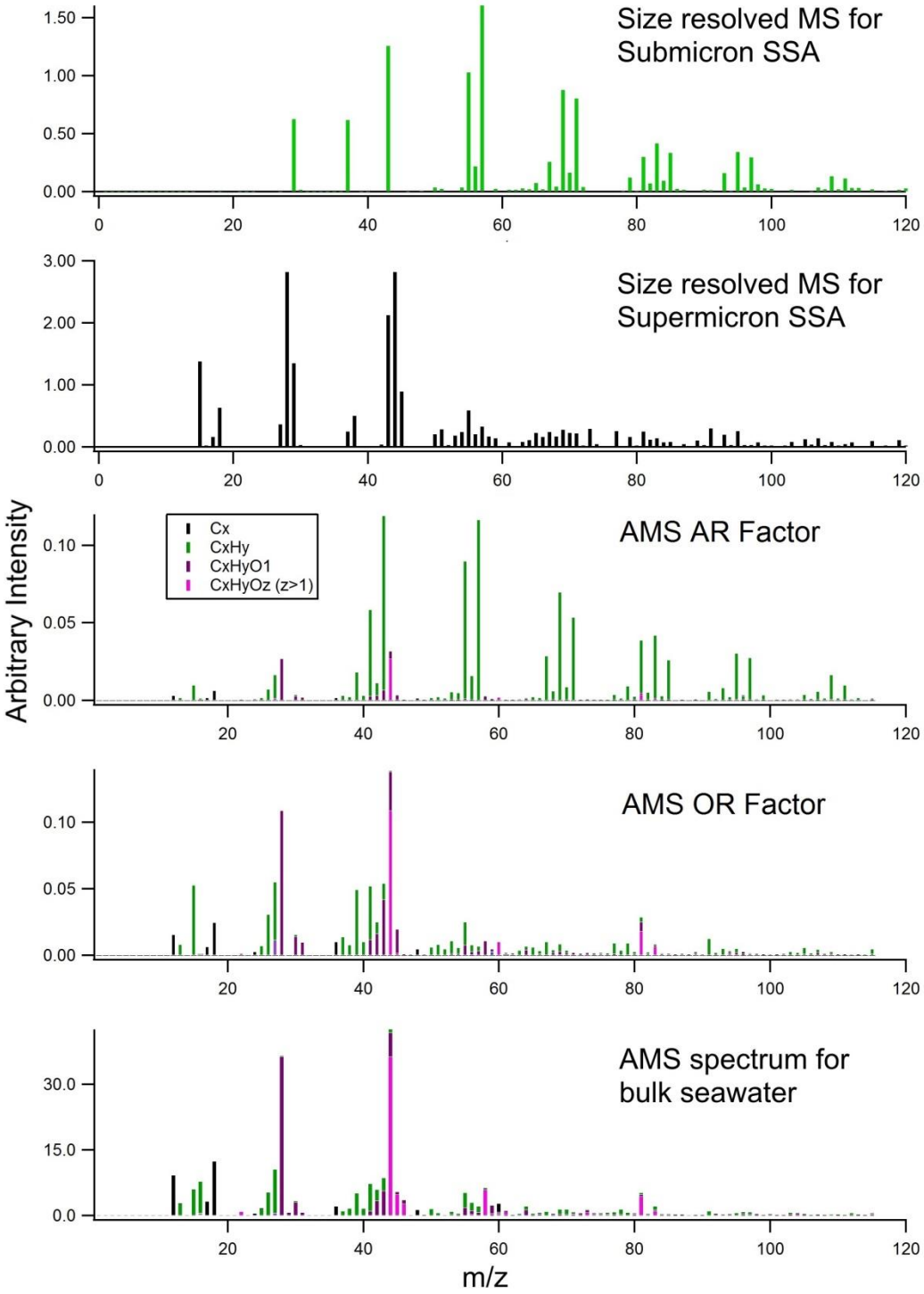

Figure S4. Elemental ratios of organics in SSA, calculated from the high resolution AMS mass spectra (C: carbon, H: hydrogen, and O: oxygen).

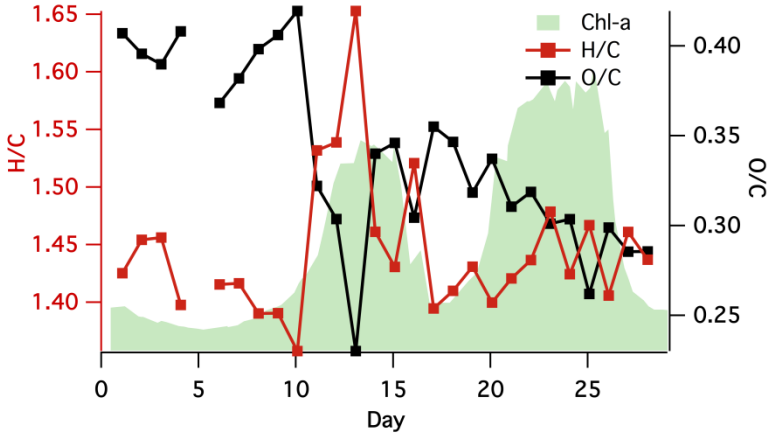

Figure S5. (A) ATOFMS spectra (weight matrices) and (B) size (D_{va}) resolved number fraction of the SSOC and OC SSA types from the wave channel experiment. The mass spectra for particles designated as OC are dominated by ion signals from organic species and magnesium and potassium as well. However, the relative ion intensity from sodium is <1% of that observed in SSOC particles. In contrast, particles classified as SSOC yield mass spectra with strong signals from NaCl ion markers, as well as enrichment in organic species and biological markers relative to particles defined as sea salt.[3]

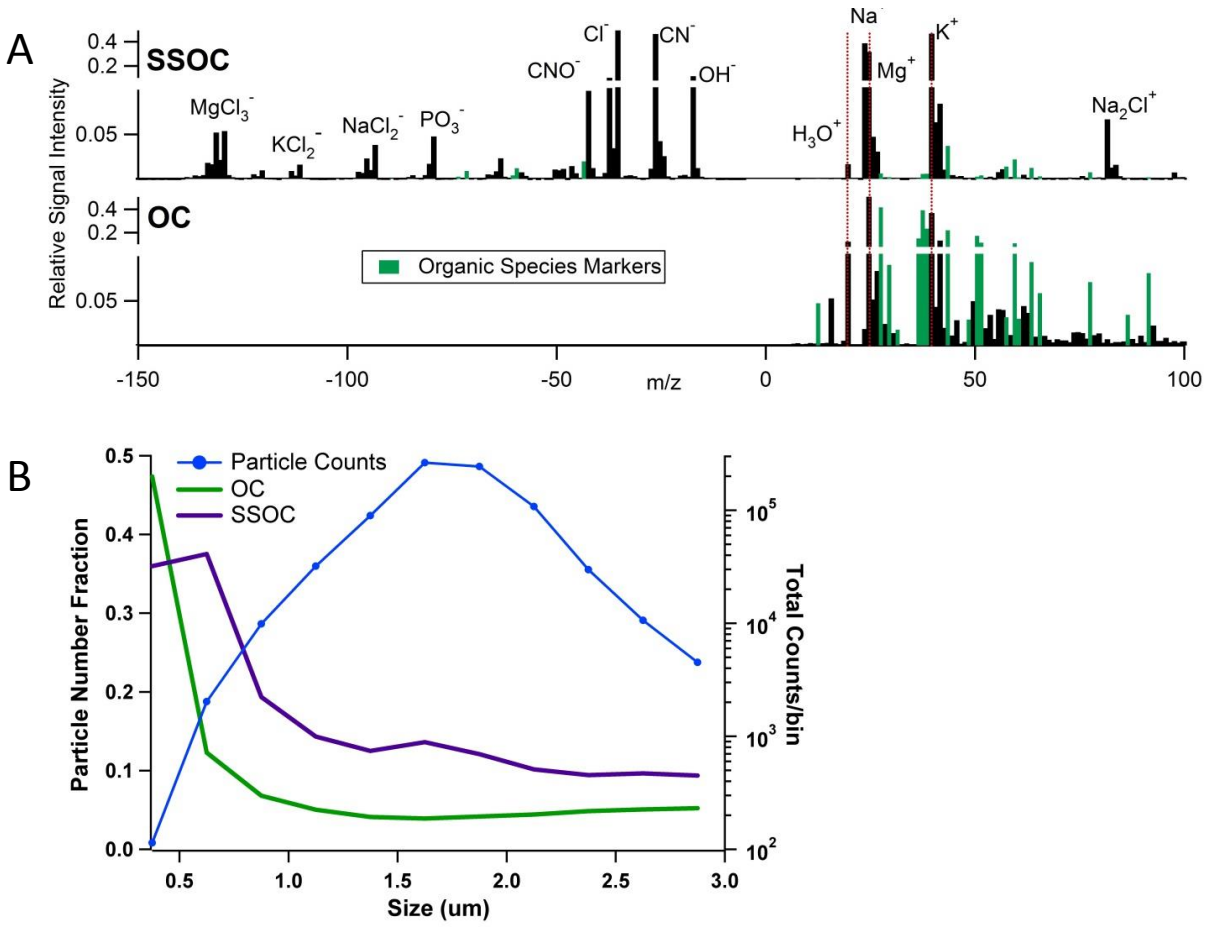

Figure S6. Representative Raman spectra of SSA particles and assignments to the vibrational peaks are provided in each table. Peaks marked with an asterisk in each spectrum are due to the quartz substrate (Method S9).

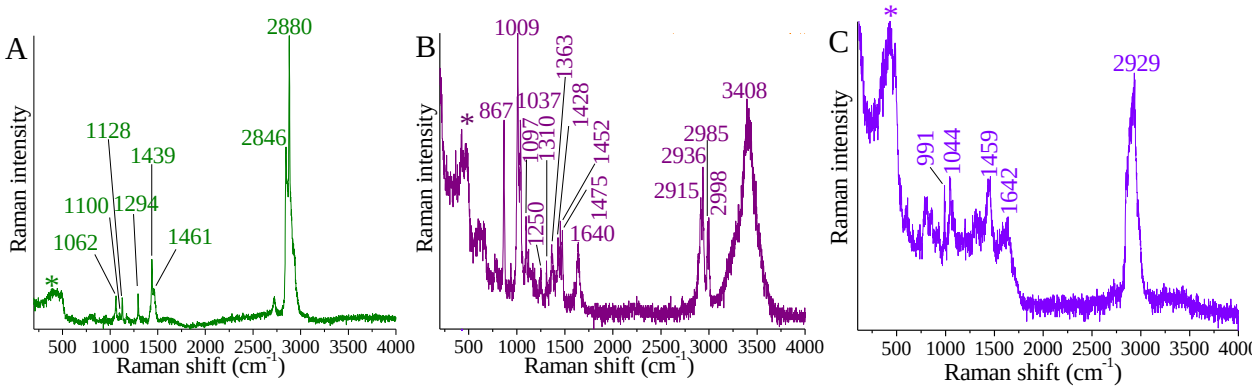

Raman shift, cm^{-1}	Assignment
1062, 1100, 1128	υ(C-C)
1294, 1439, 1461	δ(CH_2)
2846	υ_s(CH_2)
2880	υ_{as}(CH_2)

Raman shift, cm^{-1}	Assignment
867	δ(COH)
1009, 1037, 1097	υ(C–O) and υ(C–C)
1310, 1363, 1428, 1452, 1475	δ(CH_2) and δ (CH_2OH)
1250, 1640	amide III and I bands
2915, 2936, 2985, 2998	υ(C-H)
3408	υ(O-H)

Raman shift, cm^{-1}	Assignment
991, 1044	υ(C-C), υ(C-O) and υ(C-C-O)
1459	δ(CH_2)
1642	amide I band overlapping with υ(C=C)
2929	υ(C–H)

Low O/C

High O/C

Figure S7. Measured enzyme activity of the bulk seawater with target sites of the substrates given in parentheses where necessary (Method S5).

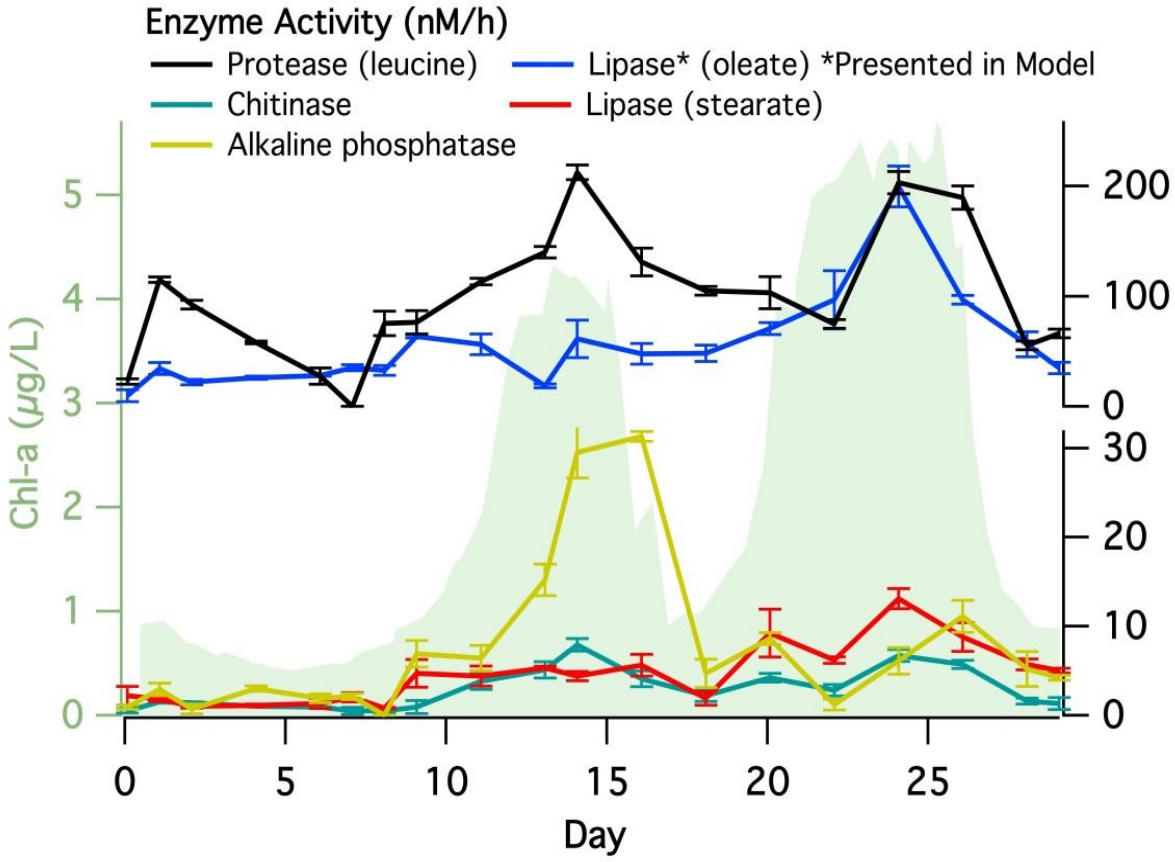

Figure S8. Average mass size distribution (calculated from the particle number size distribution, Method S6) of SSA produced from the wave channel over the entire experiment.

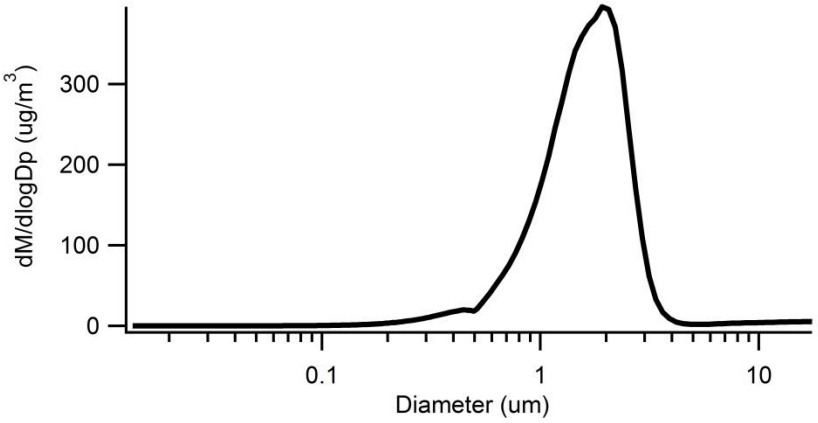

References:

1. Lee, C., Sultana, C. M., Collins, D. B., Santander, M. V., Axson, J. L., Malfatti, F., Cornwell, G. C., Grandquist, J. R., Deane, G. B., Stokes, M. D., Azam, F., Grassian, V. H., and Prather, K. A. (2015) Reproducing the chemical complexity of sea spray aerosols in a laboratory setting, *Submitted*.

2. Collins, D. B., Zhao, D. F., Ruppel, M. J., Laskina, O., Grandquist, J. R., Modini, R. L., Stokes, M. D., Russell, L. M., Bertram, T. H., Grassian, V. H., Deane, G. B., and Prather, K. A. (2014) Direct aerosol chemical composition measurements to evaluate the physicochemical differences between controlled sea spray aerosol generation schemes, *Atmos. Meas. Tech. 7*, 3667-3683.

3. Prather, K. A., Bertram, T. H., Grassian, V. H., Deane, G. B., Stokes, M. D., DeMott, P. J., Aluwihare, L. I., Palenik, B. P., Azam, F., Seinfeld, J. H., Moffet, R. C., Molina, M. J., Cappa, C. D., Geiger, F. M., Roberts, G. C., Russell, L. M., Ault, A. P., Baltrusaitis, J., Collins, D. B., Corrigan, C. E., Cuadra-Rodriguez, L. A., Ebben, C. J., Forestieri, S. D., Guasco, T. L., Hersey, S. P., Kim, M. J., Lambert, W. F., Modini, R. L., Mui, W., Pedler, B. E., Ruppel, M. J., Ryder, O. S., Schoepp, N. G., Sullivan, R. C., and Zhao, D. F. (2013) Bringing the ocean into the laboratory to probe the chemical complexity of sea spray aerosol, *Proc. Natl. Acad. Sci. U. S. A. 110*, 7550-7555.

4. Noble, R. T., and Fuhrman, J. A. (1998) Use of SYBR Green I for rapid epifluorescence counts of marine viruses and bacteria, *Aquatic. Microbial. Ecology 14*, 113-118.

5. Hoppe, H. G. (1983) Significance of exoenzymatic activities in the ecology of brackish water – measurements by means of methylumbelliferyl-substrates, *Marine Ecology Progress Series 11*, 299-308.

6. Martinez, J., Smith, D. C., Steward, G. F., and Azam, F. (1996) Variability in ectohydrolytic enzyme activities of pelagic marine bacteria and its significance for substrate processing in the sea, *Aquat. Microb. Ecol. 10*, 223-230.

7. Danovaro, R., Armeni, M., Luna, G. M., Corinaldesi, C., Dell'Anno, A., Ferrari, C. R., Fiordelmondo, C., Gambi, C., Gismondi, M., Manini, E., Mecozzi, M., Perrone, F. M., Pusceddu, A., and Giani, M. (2005) Exo-enzymatic activities and dissolved organic pools in relation with mucilage development in the Northern Adriatic Sea, *Sci. Total Environ. 353*, 189-203.

8. Zelenyuk, A., Imre, D., Cuadra-Rodriguez, L. A., and Ellison, B. (2007) Measurements and interpretation of the effect of a soluble organic surfactant on the density, shape and water uptake of hygroscopic particles, *J. Aerosol. Sci. 38*, 903-923.

9. Neubauer, K. R., Johnston, M. V., and Wexler, A. S. (1997) On-line analysis of aqueous aerosols by laser desorption ionization, *Int. J. Mass Spectrom. Ion Processes 163*, 29-37.

10. Noble, C. A., and Prather, K. A. (1996) Real-time measurement of correlated size and composition profiles of individual atmospheric aerosol particles, *Environ. Sci. Technol. 30*, 2667-2680.

11. Gard, E., Mayer, J. E., Morrical, B. D., Dienes, T., Fergenson, D. P., and Prather, K. A. (1997) Real-time analysis of individual atmospheric aerosol particles: Design and performance of a portable ATOFMS, *Anal. Chem. 69*, 4083-4091.

12. Song, X. H., Hopke, P. K., Fergenson, D. P., and Prather, K. A. (1999) Classification of single particles analyzed by ATOFMS using an artificial neural network, ART-2A, *Anal. Chem. 71*, 860-865.

13. DeCarlo, P. F., Kimmel, J. R., Trimborn, A., Northway, M. J., Jayne, J. T., Aiken, A. C., Gonin, M., Fuhrer, K., Horvath, T., Docherty, K. S., Worsnop, D. R., and Jimenez, J. L. (2006) Field-Deployable, High-Resolution, Time-of-Flight Aerosol Mass Spectrometer, *Anal. Chem. 78*, 8281-8289.

14. Jayne, J. T., Leard, D. C., Zhang, X. F., Davidovits, P., Smith, K. A., Kolb, C. E., and Worsnop, D. R. (2000) Development of an aerosol mass spectrometer for size and composition analysis of submicron particles, *Aerosol Sci. Technol. 33*, 49-70.

15. Liu, P. S. K., Deng, R., Smith, K. A., Williams, L. R., Jayne, J. T., Canagaratna, M. R., Moore, K., Onasch, T. B., Worsnop, D. R., and Deshler, T. (2007) Transmission Efficiency of an Aerodynamic Focusing Lens System: Comparison of Model Calculations and Laboratory Measurements for the Aerodyne Aerosol Mass Spectrometer, *Aerosol Sci. Technol. 41*, 721-733.

16. Aiken, A. C., DeCarlo, P. F., and Jimenez, J. L. (2007) Elemental Analysis of Organic Species with Electron Ionization High-Resolution Mass Spectrometry, *Anal. Chem. 79*, 8350-8358.

17. Hämeri, K., Laaksonen, A., Väkevä, M., and Suni, T. (2001) Hygroscopic growth of ultrafine sodium chloride particles, *J. Geophys. Res.-Atmos. 106*, 20749-20757.

18. Paatero, P., and Tapper, U. (1994) Positive matrix factorization: A non-negative factor model with optimal utilization of error estimates of data values, *Environmetrics 5*, 111-126.

19. Ulbrich, I. M., Canagaratna, M. R., Zhang, Q., Worsnop, D. R., and Jimenez, J. L. (2009) Interpretation of organic components from Positive Matrix Factorization of aerosol mass spectrometric data, *Atmos. Chem. Phys. 9*, 2891-2918.

20. De Gelder, J., De Gussem, K., Vandenabeele, P., and Moens, L. (2007) Reference database of Raman spectra of biological molecules, *J. Raman Spectrosc. 38*, 1133-1147.

21. Hill, I. R., and Levin, I. W. (1979) Vibrational spectra and carbon hydrogen stretching mode assignments for a series of normal alkyl carboxylic acids, *J. Chem. Phys. 70*, 842-851.

22. Gomes, H., Rosina, P., Holakooei, P., Solomon, T., and Vaccaro, C. (2013) Identification of pigments used in rock art paintings in Gode Roriso-Ethiopia using Micro-Raman spectroscopy, *J. Archaeol. Sci. 40,* 4073-4082.

23. Spiker, R. C., and Levin, I. W. (1975) Raman spectra and vibrational assignments for dipalmitoyl phosphatidylcholine and structurally related molecules, *Biochim. Biophys. Acta. 388,* 361-373.

24. Pemberton, J. E., and Chamberlain, J. R. (2000) Raman spectroscopy of model membrane monolayers of dipalmitoylphosphatidic acid at the air-water interface using surface enhancement from buoyant thin silver films, *Biopolymers 57,* 103-116.

25. She, C. Y., and Tu, A. T. (1974) Laser Raman scattering of glucosamine N-acetylglucosamine, and glucuronic acid, *Biochim. Biophys. Acta. 372*, 345-357.

26. Wu, H., Volponi, J. V., Oliver, A. E., Parikh, A. N., Simmons, B. A., and Singh, S. (2011) In vivo lipidomics using single-cell Raman spectroscopy, *Proc. Natl. Acad. Sci. U. S. A. 108*, 3809-3814.

27. Amharref, N., Bejebbar, A., Dukie, S., Venteo, L., Schneider, L., Pluot, M., and Manfait, M. (2007) Discriminating healthy from tumor and necrosis tissue in rat brain tissue samples by Raman spectral imaging, *Biochim. Biophys. Acta.-Biomembranes 1768,* 2605-2615.

28. Lin, V. J. C., and Koenig, J. L. (1976) Raman studies of bovine serum albumin, *Biopolymers 15*, 203-218.

29. Compiano, A. M., Romano, J. C., Garabetian, F., Laborde, P., and Delagiraudiere, I. (1993) Monosaccharide compostion of particulate hydrolyzable sugar fraction in surface microlayers from brackish and marine waters, *Mar. Chem. 42*, 237-251.

30. Russell, L. M., Hawkins, L. N., Frossard, A. A., Quinn, P. K., and Bates, T. S. (2010) Carbohydrate-like composition of submicron atmospheric particles and their production from ocean bubble bursting, *Proc. Natl. Acad. Sci. U. S. A. 107*, 6652-6657.

31. Hawkins, L. N., and Russell, L. (2010) Polysaccharides, Proteins, and Phytoplankton Fragments: Four Chemically Distinct Types of Marine Primary Organic Aerosol Classified by Single Particle Spectromicroscopy, *Advances in Meteorology*. 612132, DOI: 10.1155/2010/612132

32. Gao, Q., Leck, C., Rauschenberg, C., and Matrai, P. A. (2012) On the chemical dynamics of extracellular polysaccharides in the high Arctic surface microlayer, *Ocean Sci. 8*, 401-418.

33. van Pinxteren, M., Müller, C., Iinuma, Y., Stolle, C., and Herrmann, H. (2012) Chemical Characterization of Dissolved Organic Compounds from Coastal Sea Surface Microlayers (Baltic Sea, Germany), *Environ. Sci. Technol. 46*, 10455-10462.

34. Cunliffe, M., Engel, A., Frka, S., Gasparovic, B., Guitart, C., Murrell, J. C., Salter, M., Stolle, C., Upstill-Goddard, R., and Wurl, O. (2013) Sea surface microlayers: A unified physicochemical and biological perspective of the air-ocean interface, *Prog. Oceanogr. 109*, 104-116.

35. Laucks, M. L., Sengupta, A., Junge, K., Davis, E. J., and Swanson, B. D. (2005) Comparison of psychro-active arctic marine bacteria and common mesophillic bacteria using surface-enhanced Raman spectroscopy, *Appl. Spectrosc. 59*, 1222-1228.

36. Kamnev, A. A., Tarantilis, P. A., Antonyuk, L. P., Bespalova, L. A., Polissiou, M. G., Colina, M., Gardiner, P. H. E., and Ignatov, V. V. (2001) Fourier transform Raman spectroscopic characterisation of cells of the plant-associated soil bacterium Azospirillum brasilense Sp7, *J. Mol. Struct. 563*, 199-207.

37. Carlson, R. W., Kalembasa, S., Turowski, D., Pachori, P., and Noel, K. D. (1987) Characterization of the lipopolysaccharide from a Rhizobium Phaseoli mutant that is defective in infection thread development, *J. Bacteriol. 169*, 4923-4928.

38. Weckesser, J., Drews, G., and Fromme, I. (1972) Chemical analysis of and degradation studies on cell wall lipopolysaccharide of Rhodopseudomonas capsulata, *J. Bacteriol. 109*, 1106.

39. Vali, G. (1971) Quantitative Evaluation of Experimental Results an the Heterogeneous Freezing Nucleation of Supercooled Liquids, *J. Atmos. Sci. 28*, 402-409.

40. Agresti, A., and Coull, B. A. (1998) Approximate Is Better than "Exact" for Interval Estimation of Binomial Proportions, *The American Statistician 52*, 119-126.

41. Canagaratna, M. R., Jayne, J. T., Jimenez, J. L., Allan, J. D., Alfarra, M. R., Zhang, Q., Onasch, T. B., Drewnick, F., Coe, H., Middlebrook, A., Delia, A., Williams, L. R., Trimborn, A. M., Northway, M. J., DeCarlo, P. F., Kolb, C. E., Davidovits, P., and Worsnop, D. R. (2007) Chemical and microphysical characterization of ambient aerosols with the aerodyne aerosol mass spectrometer, *Mass Spectrom. Rev. 26*, 185-222.

42. Ratte, M., Plass-Dulmer, C., Koppmann, R., and Rudolph, J. (2011) Horizontal and vertical profiles of light hydrocarbons in sea water related to biological, chemical and physical parameters, *Tellus B 47*. 607-623